# ELECTRON MICROSCOPY OF SERPENTINITE TEXTURES

B.A. CRESSEY*

*Department of Geology, University of Manchester, Manchester, U.K. M13 9PL*

## ABSTRACT

Electron microscopy of ion-thinned samples of serpentinites has been used to study the structures and morphologies of common serpentine textures in rocks from various locations and geological environments. Electron diffraction and electron-optical observations are correlated with the light-optical and X-ray data obtained by previous workers. In pseudomorphic textures, apparently fibrous $\alpha$–serpentine is shown to consist of parallel stacks of lizardite plates, $\gamma$–serpentine fibres are true chrysotile fibres, and apparently nonfibrous serpentine generally consists of poorly crystalline, randomly oriented, fine-grained mixtures of lizardite, chrysotile and polygonal serpentine (which has been identified as Povlen-type chrysotile). In non-pseudomorphic textures $\gamma$-serpentine is antigorite or a mixture of chrysotile, polygonal serpentine and lizardite in varying proportions. The appearance and distribution of well-crystallized, well-oriented serpentine and poorly crystalline, randomly oriented serpentine in pseudomorphic textures are interpreted as being formed by the relatively rapid replacement of preserpentinization minerals by poorly formed serpentine, often followed by recrystallization (partial or complete) of this serpentine to a more coarsely crystalline, well-oriented form. For example, in mesh textures where apparently fibrous lizardite surrounds poorly formed serpentine, the centre represents the initial serpentine formed and the mesh rims, subsequent recrystallization.

## SOMMAIRE

Nous avons étudié, par microscopie électronique d'échantillons de serpentinite préalablement amincis sous ions, la structure et la morphologie de textures de serpentine commune, dans des roches provenant de diverses localités de cadres géologiques différents. Nous faisons la corrélation entre nos observations par microscopie et diffraction électroniques et les résultats que des auteurs précédents ont obtenus par les méthodes des rayons X et de l'optique en lumière visible. Nous montrons que, dans les textures pseudomorphes, la serpentine–$\alpha$ fibreuse en apparence consiste en empilements parallèles de plaquettes de lizardite, les fibres de serpentine–$\gamma$ sont des fibres de chrysotile, et la serpentine non-fibreuse en apparence consiste généralement en mélanges de grains très petits, mal cristallisés, sans orientation privilégiée, de lizardite, chrysotile et serpentine polygonale (identifiée comme chrysotile de type Povlen). Dans les textures non-pseudomorphes, la serpentine–$\gamma$ est de l'antigorite ou bien un mélange de chrysotile, serpentine polygonale et lizardite en proportions variables. L'aspect et la distribution de serpentine bien cristallisée, bien orientée, et de serpentine à cristallinité médiocre, non-orientée, dans les textures pseudomorphes, s'explique par le remplacement relativement rapide des minéraux antérieurs à la serpentinisation par de la serpentine mal formée qui, dans une recristallisation ultérieure (partielle ou totale) aurait fréquemment donné une forme à grain plus grossier bien orienté. Exemple: dans les textures à mailles où la lizardite fibreuse en apparence entoure de la serpentine mal formée, le centre représente la serpentinisation initiale et la bordure maillée, la recristallisation.

(Traduit par la Rédaction)

## INTRODUCTION

Previous studies of textures in serpentinites have utilized X-ray-diffraction techniques and optical microscopy. The very fine-grained nature of these minerals presents problems for the latter approach, and with X-ray powder methods there is no way of relating the information obtained to the textures observed in the rock. Using an X-ray-microbeam camera, however, Wicks (1969), Wicks & Zussman (1975), Wicks *et al.* (1977) and Wicks & Whittaker (1977) succeeded, to a great extent, in determining 1) the mineralogy of the textures and 2) the relationship between the orientations of the crystals in the textural units and their optical properties.

Ion-thinning (Barber 1970, Champness & Lorimer 1971) has proved to be a particularly useful method of sample preparation for electron-microscopy studies of serpentinites (Cressey & Zussman 1976, Cressey 1977). This technique permits the study of mineral grains in the orientations and with the spatial relationships in which they were formed in the rock. Since

the ion-thinned specimen is taken from a normal thin-section prepared as for optical microscopy, a direct correlation can be made between the information from electron optics and light optics.

The purpose of this study is the correlation of electron–optics observations on serpentinites with optical and X-ray data obtained by Wicks (1969), Wicks & Zussman (1975) and Wicks & Whittaker (1977). Electron microscopy can thus be used to provide direct, visual evidence concerning structures inferred from X-ray data, and also to provide additional details that cannot be obtained using other techniques. Interpretation of the electron-optics observations provides a valuable contribution towards our understanding of the serpentinization process.

## DESCRIPTION OF SPECIMENS

Specimens were kindly provided by the Department of Geology and Mineralogy, University of Oxford; they were selected as examples of the common serpentinite textures from a variety of locations and geological settings. They had been previously studied by optical microscopy and by microbeam X-ray techniques by Wicks (1969), Wicks & Zussman (1975) and Wicks & Whittaker (1977), and the brief descriptions given below and in a previous publication (Cressey & Zussman 1976) are based on their observations. In many of the specimens the mineralogy and textures are complex and some of the specimens are inhomogeneous. The notations used here for the serpentine polymorphs are those of Wicks & Whittaker (1975).

### Serpentinites with pseudomorphic textures

Specimens 18505, 18508, 18527 and 18540 have been previously described by Cressey & Zussman (1976). Specimen 18509, a serpentinized amphibole peridotite from Glen Urquhart, Scotland, consists mainly of lizardite–1T in $\alpha$-serpentine mesh-texture and amphibole bastites. The latter consist of $\alpha$, $\gamma$ and isotropic serpentine, commonly with relict amphibole. The mesh textures often contain relict olivine in the mesh centres. Specimen 18510, a serpentinized peridotite from the Lizard (Cornwall, England), consists of lizardite–1T in $\alpha$-mesh texture and $\gamma$-serpentine bastites after pyroxenes (mainly orthopyroxene). In the orthopyroxene bastites serpentinization has been almost complete, but some narrow clinopyroxene lamellae remain unaltered. In the clinopyroxene bastites much of the clinopyroxene is unaltered, whereas the

orthopyroxene has been almost entirely replaced by serpentine. The mesh textures may contain relict olivine in the mesh centres. The specimen also contains small amounts of chromite.

### Serpentinites with pseudomorphic textures that have begun to transform to non-pseudomorphic textures

Specimens 18500 and 18501 have been previously described by Cressey & Zussman (1976).

### Serpentinites with non-pseudomorphic textures

Specimens 18541 and 18543 have been previously described by Cressey & Zussman (1976). Specimen 18523, a serpentinite from Tasiussarssuaq Fjord, Greenland, consists of antigorite in $\gamma$-serpentine interpenetrating textures. The specimen also contains various opaque minerals. Specimen 18558, a serpentinite from Knee Lake, Manitoba, consists of antigorite in apparent $\gamma$-hourglass and interpenetrating textures, with several opaque minerals.

### Serpentine veins

Specimens 18515 and 18536 have been previously described by Cressey & Zussman (1976).

## PSEUDOMORPHIC TEXTURES

### Mesh textures

Mesh textures in both partly serpentinized and completely serpentinized rocks have been examined. All except one (18501) consist mainly of lizardite. In these, lizardite mesh-rims consists of apparent fibres of lizardite–1T that lie approximately parallel to one another, perpendicular to the rim walls (Figs. 1a, 2a). These apparent fibres are stacks of lizardite plates; the stacks are polygonal in cross-section (Fig. 3) and have z parallel to the apparent-fibre axis (Fig. 2a). The apparent fibres range from about 0.1 to 1 $\mu$m in width, though this is often variable along the length as the edges of the stacks are commonly sinuous or crenulated. Between adjacent stacks there is often a gap of up to about 0.05 $\mu$m in width; it seems to be filled with very fine grained material. Electron diffraction indicates that there is little rotation about the z axis between adjacent stacks of plates; within one mesh rim almost all the apparent fibres lie with the same crystallographic axis parallel to the electron beam. Wicks & Zussman (1975) have reported that the micro-
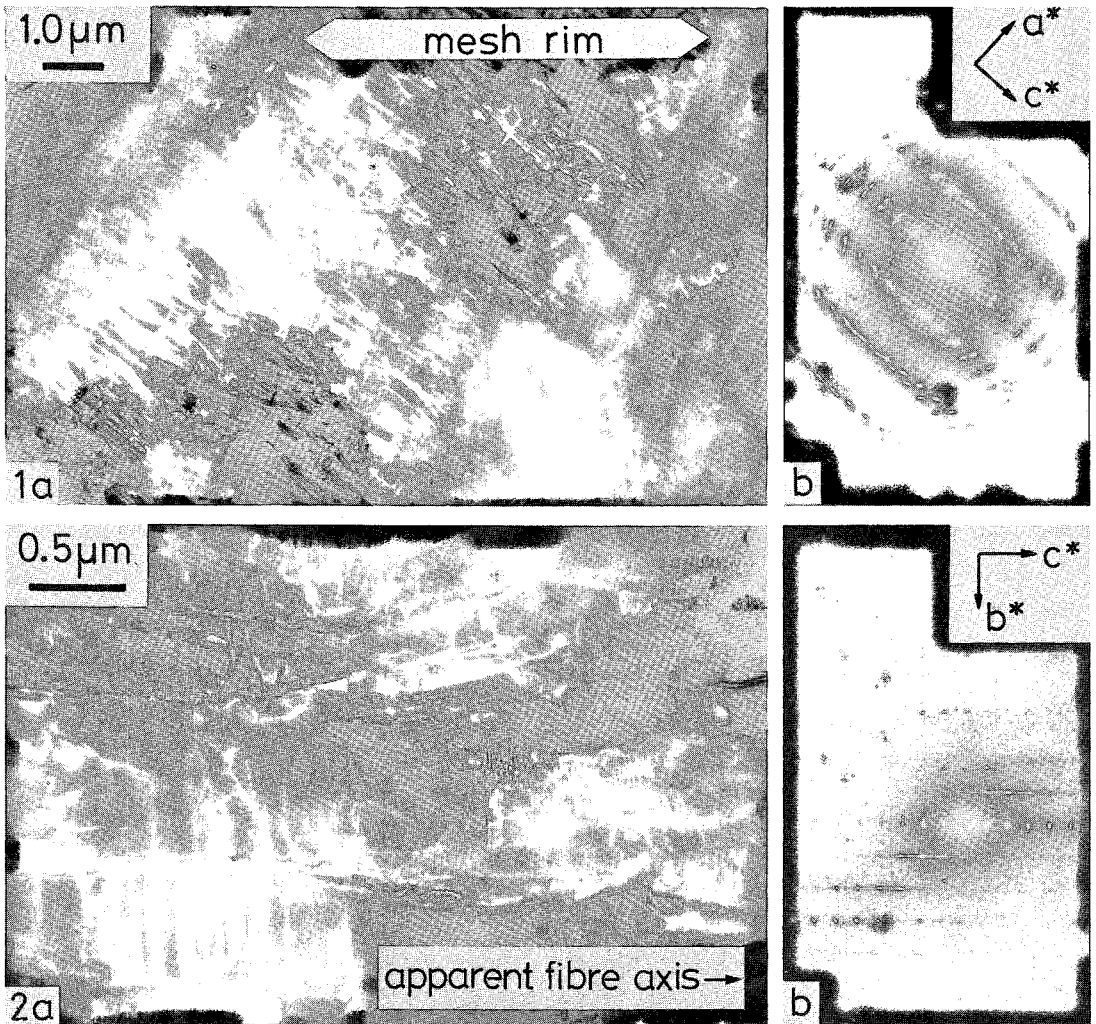
FIG. 1.(a) Lizardite ($\alpha$-serpentine) mesh-rim. Specimen 18527. (b) Selected-area diffraction pattern from the mesh rim in (a).

FIG. 2.(a) Lizardite apparent-fibres forming an $\alpha$-serpentine mesh-rim. Specimen 18505. (b) Selected-area diffraction pattern from the mesh rim in (a).

beam X-ray-diffraction pattern produced when the microbeam is parallel to the apparent-fibre axis indicates a strong crystallographic continuity, within 30 to 40° of arc, between the adjacent apparent fibres. However, groups of apparent fibres may be slightly fanned, so that individual apparent-fibres may have their z axes up to 10° or so from the average z-axis direction within the rim (Fig. 1b). The X-ray studies of Wicks & Zussman (1975) also indicated this fanning of z axes in $\alpha$-serpentine fibres. A stacking disorder with a fault vector $R = \pm b/3$ is almost always present in mesh-rim lizardite;

the probability that a fault will occur is generally about 0.5, but can be almost zero. This was also observed in X-ray-diffraction patterns of a lizardite crystal studied by Rucklidge & Zussman (1965). This stacking disorder is evident in selected-area electron-diffraction patterns such as that shown in Figure 2b. Most grains in this orientation show patterns of high and irregular contrast. Rucklidge & Zussman (1965) reported that platy lizardite grains are bent about $x$ and $y$ axes; the high-contrast patterns shown by many of these grains could be caused by such buckling.
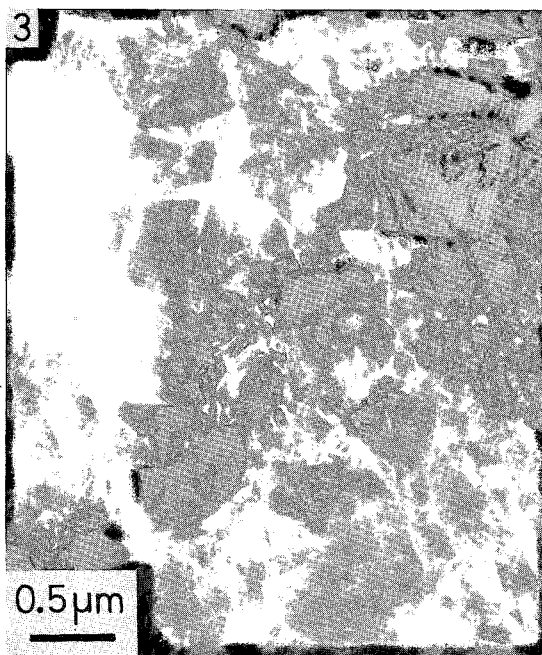
FIG. 3. Cross-sections of lizardite (α-serpentine) mesh-rim apparent-fibres (*i.e.*, electron beam is parallel to *c**). Specimen 18509.
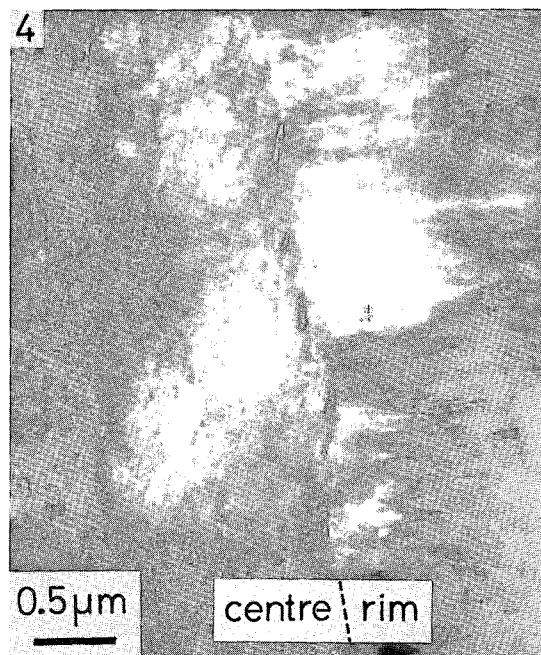
FIG. 4. Rim–centre boundary in an α-serpentine mesh-texture. Specimen 18505.

Central partings in mesh rims, seen in the optical micrographs as isotropic' serpentine, can in some cases be observed in the electron microscope. They are generally about 1 to 2 μm in width and seem to consist of very fine grained serpentine, probably lizardite, though it is difficult to determine this by electron diffraction since the patterns produced by this material are weak and resemble diffuse powder-rings.

Mesh centres in all specimens except 18501 consist of fine-grained, randomly oriented serpentine, and the rim–centre boundary is sharp and fairly straight (Fig. 4). This serpentine seems to be mainly lizardite, but chrysotile and polygonal serpentine (Cressey & Zussman 1976) are generally also present (Fig. 5). In specimen 18505 many mesh centres also contain large, platy or elongate grains of brugnatellite intergrown with the serpentine (Fig. 6). The brugnatellite grains bear no relationship in orientation or distribution to the geometry of the mesh cell. In specimen 18527 many mesh centres are outlined by magnetite, and in the electron microscope strings of small magnetite grains can be seen in the fine-grained serpentine close to mesh rims and running parallel to them. Because magnetite is much more resistant to ion-

thinning than serpentine, these grains are always too thick to be transparent to electrons, but can be recognized by their characteristic diamond or octahedral shapes. The magnetite grains do not seem related in any way to the habits, orientations or distributions of chrysotile and lizardite.

In specimens 18509 and 18510, many mesh centres contain relict olivine. Because of the difference in thinning rates between olivine and serpentine, it was very difficult to obtain thinned areas in which the olivine–serpentine boundary could be examined. In spite of this difficulty, a few suitably thinned samples were produced. The boundaries are generally irregular in shape and commonly embayed. The serpentine adjacent to these boundaries is usually very fine-grained and in random orientations, (Fig. 7), which produce ring-type electron-diffraction patterns and therefore cannot be identified more precisely. In only one place has well-oriented, well-crystallized serpentine (lizardite–1*T*) been found adjacent to olivine, and here the serpentine appears very much like that in other lizardite mesh-rims, with apparent fibres roughly perpendicular to the olivine–serpentine boundary, which is fairly straight (Fig. 8). The crystallographic orientation of the ol-
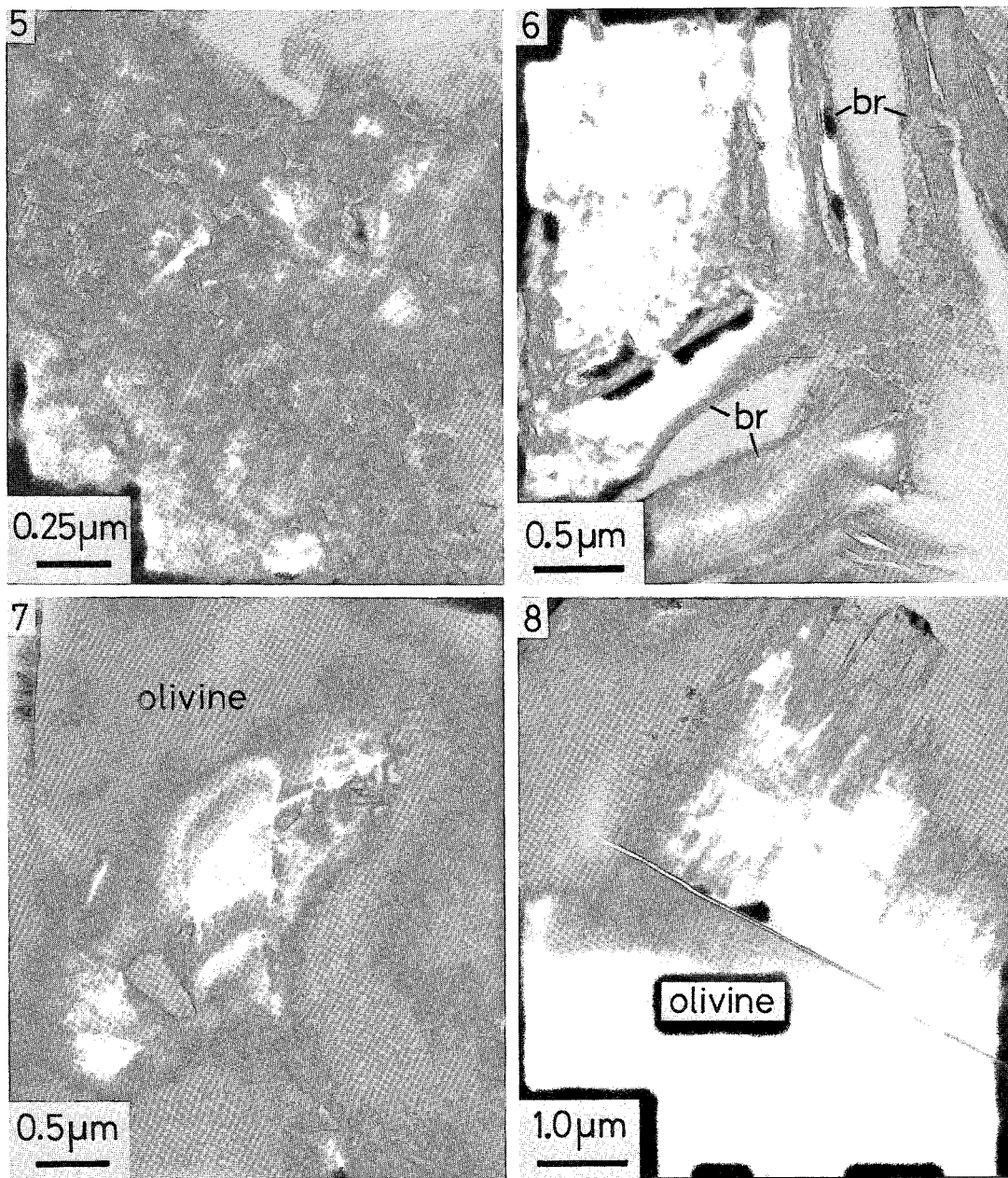
FIG. 5. Randomly oriented, poorly formed lizardite, chrysotile and polygonal serpentine fibres in a mesh centre from an $\alpha$-serpentine mesh-texture. Specimen 18505.

FIG. 6. Brugnatellite (br) intergrown with serpentine in a mesh centre from an $\alpha$-serpentine mesh-texture. Specimen 18505.

FIG. 7. An olivine–serpentine boundary in an $\alpha$-serpentine mesh texture. The serpentine is fine-grained and randomly oriented. Specimen 18510.

FIG. 8. An olivine–serpentine boundary in an $\alpha$-serpentine mesh-texture. The serpentine is well-formed, well-oriented lizardite, as in Fig. 2, with $c^*$ perpendicular to the boundary with olivine. Specimen 18510.

ivine does not appear related to that of the serpentine, even where the latter is well crystallized. However, in optical micrographs serpentine mesh-rims around olivine are quite irregular in shape, and do not necessarily follow along olivine planes with simple indices. The well-oriented, well-crystallized lizardite occurs (though apparently only rarely) along major grain-boundaries, whereas the poorly crystalline, randomly oriented serpentine lies along most boundaries and in embayments and irregular cracks running through the olivine grains.

One chrysotile mesh-texture (18501) was examined. The rims consist of parallel chrysotile–

$2M_{c1}$ fibres, with fibre axes ($x$) perpendicular to the rim walls. The mesh centres are randomly oriented chrysotile–$2M_{c1}$ fibres and polygonal serpentine (Cressey & Zussman 1976, p. 309, Figs. 1, 3). The boundary between the rims and centres is distinct and fairly straight, similar to lizardite mesh-textures. A more detailed description of electron-microscope observations on this specimen has already been published (Cressey & Zussman 1976).

*Hourglass textures*

As was expected, hourglass textures (18500
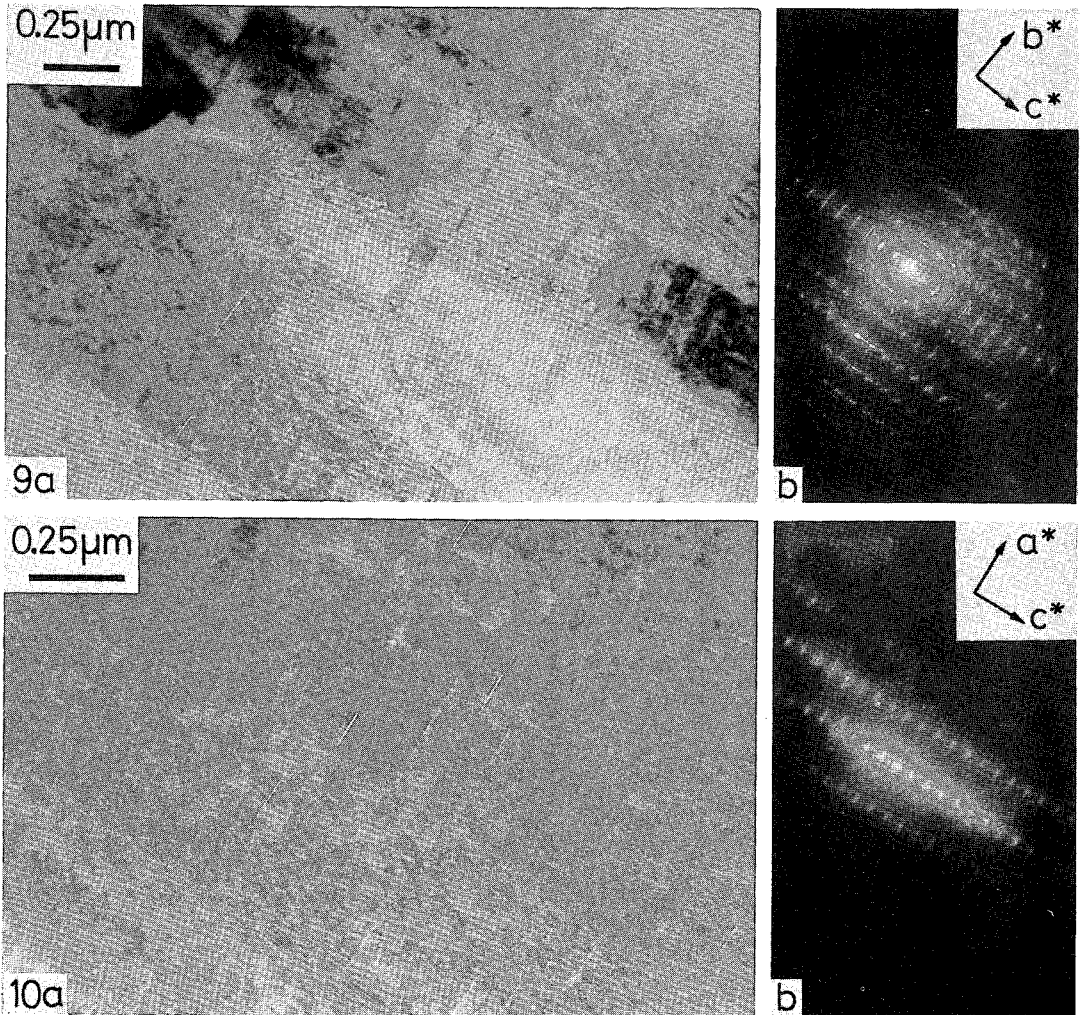




FIG. 9. (a) Hourglass texture sectioned perpendicular to the $x$ axis. Specimen 18540. (b) Selected-area diffraction pattern from the area in (a).

FIG. 10. (a) Hourglass texture sectioned perpendicular to the $y$ axis. Specimen 18540. (b) Selected-area diffraction pattern from the area in (a).

and 18540) are made up mainly of lizardite–$1T$ apparent fibres; these are very similar to those forming lizardite mesh-rims, but some also contain small amounts of chrysotile between the stacks of lizardite plates. Sections perpendicular to [100] and [010] are shown in Figures 9 and 10. In this particular [100] section the regular stacking-fault with $R = \pm b/3$ is not very evident in the diffraction pattern (Fig. 9b),

but in many other parts of the specimen it is clearly present and produces diffraction patterns very similar to that shown in Figure 2b. In the [010] section diffraction spots seem to be slightly streaked in both $x$ and $z$ directions, suggesting some degree of disorder (Fig. 10b). This was found to occur quite commonly, though patterns with no streaking have also been recorded.
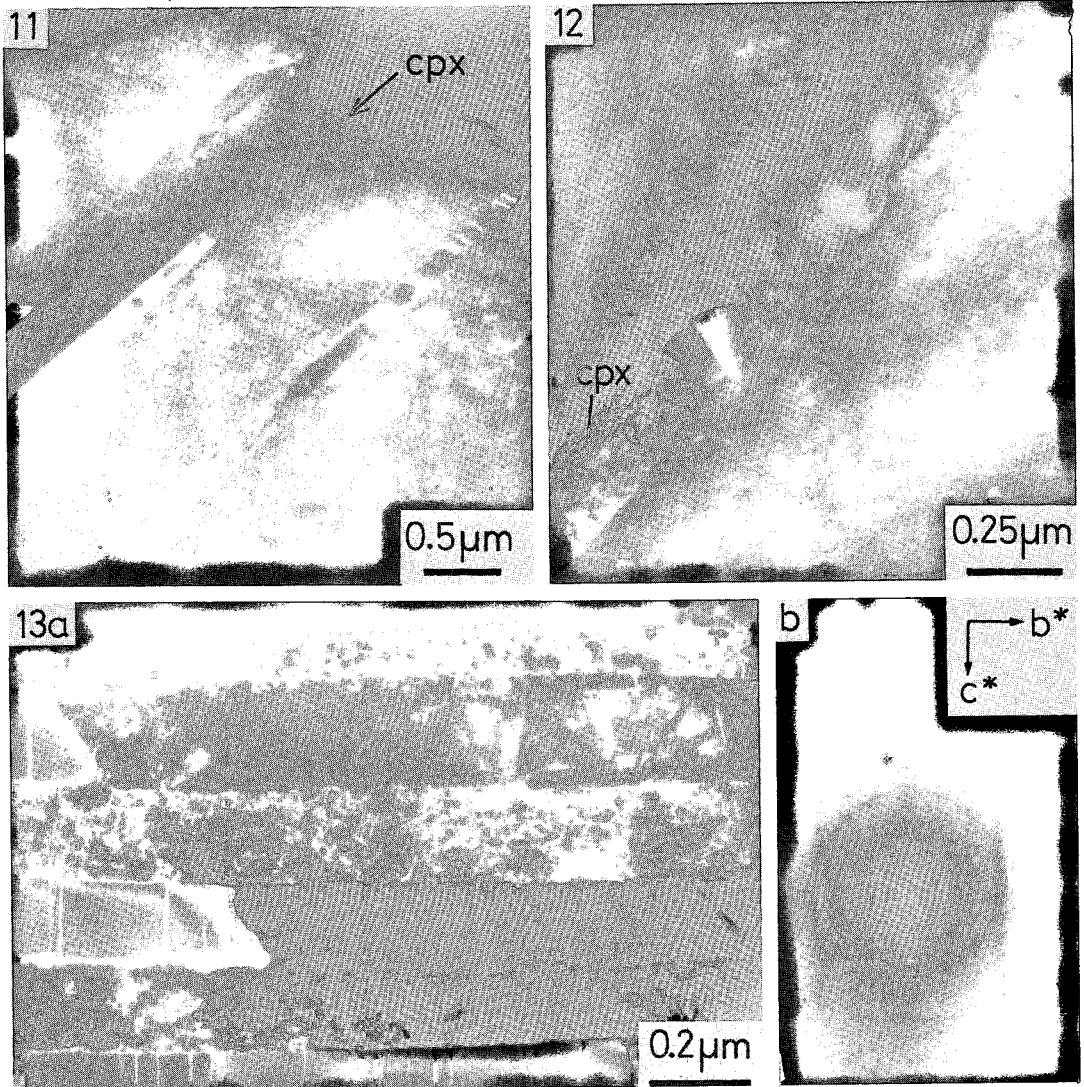
FIG. 11. Orthopyroxene bastite with unserpentinized clinopyroxene (cpx) lamellae. Specimen 18510.

FIG. 12. Orthopyroxene bastite with a partly serpentinized clinopyroxene (cpx) lamella containing polygonal serpentine. Specimen 18510.

FIG. 13.(a) Clinopyroxene bastite. Orthopyroxene has been completely serpentinized, and clinopyroxene has been partly altered. Photograph provided by P. P. K. Smith, Department of Geology, University of Manchester. (b) Selected-area diffraction pattern from the area in (a).

*Bastites*

In specimen 18510 the orthopyroxene bastites consist almost entirely of serpentine that is too fine-grained to identify. They also contain some narrow (generally 0.1 to 0.2 $\mu$m) clinopyroxene lamellae which in some samples are mainly unaltered (Fig. 11), though some pass laterally into serpentine. In other examples the clinopyroxene has been completely replaced, but the outlines of the former lamellae can still be recognized. The serpentine in the altered lamellae is often very fine grained and similar to that in the main part of the bastite, but it may also contain polygonal serpentine (Fig. 12) and poorly formed but recognizable chrysotile fibres. The polygons are always incomplete and usually have a flat diameter along one side of the lamella and the circumference touching the other side. Electron diffraction indicates that the fine-grained serpentine is almost always randomly oriented. However, the diffraction-pattern rings occasionally break into poorly developed, regular arrays of spots, indicating that the lizardite z-axis direction is roughly perpendicular to the lamellar interface, which would have been (100) in the pyroxene.

In specimen 18510, a clinopyroxene bastite in which the clinopyroxene is unaltered was also examined. Larger lamellae (0.5 to 2 $\mu$m in width), which had presumably been orthopyroxene, were found to consist entirely of serpentine, usually too fine-grained to identify, but narrow orthopyroxene lamellae (up to 0.1 $\mu$m in width) remain unaltered. The serpentine–pyroxene boundaries, though obviously following the straight orthopyroxene–clinopyroxene interface fairly closely, generally appear ragged and indistinct over a distance of up to 0.1 $\mu$m. In cases, the clinopyroxene is embayed (Fig. 11) and serpentine can break through from one lamella to the next. The serpentine in the large lamellae is generally fine-grained and randomly oriented but is sometimes more coarsely crystalline and can be identified as lizardite, though still with no very obvious relationship between serpentine and pyroxene orientations on the electron-optics scale. A sample in which the orthopyroxene has been completely altered to serpentine but in which clinopyroxene is only partly serpentinized is shown in Figure 13. Some partly serpentinized clinopyroxene lamellae contain "semicircular" sections of polygonal serpentine, similar to specimen 18510 (Fig. 12). Electron-diffraction patterns from this sample (Fig. 13b) show that although much of the fine-grained

serpentine is randomly oriented, the [100] lizardite pattern can be recognized. Thus in this specimen the approximate relationship $z_{serpentine}//x_{pyroxene}$, $y_{serpentine}//y_{pyroxene}$ and $x_{serpentine}//z_{pyroxene}$ is suggested, though the relationship is obviously not perfectly developed. X-ray studies by Wicks (1969) indicated this same relationship, again not perfectly developed, in the orthopyroxene bastites of specimen 18510. Probably the X-ray beam was diffracted by a larger area than that which produced the electron-diffraction patterns, thus showing a more representative average orientation of the serpentine.

The bastites in specimen 18500, probably after clinopyroxene, are completely serpentinized. A typical area is shown in Figure 14. Stacks of lizardite plates, similar in structure and appearance to those forming lizardite mesh-rims, run through the bastites, parallel to the lineations seen in the optical microscope. These parallel lineations may represent the cleavages or exsolution lamellae in the original pyroxene. Some groups of apparent fibres in Figure 14 occur in fanned arrangements that are very similar to those in $\alpha$-serpentine mesh-rims. Regions between stacks of plates generally consist either of very fine grained, randomly oriented serpentine that seems to be a mixture of chrysotile, lizardite and poorly formed polygonal serpentine, or, less commonly, of well-formed parallel chrysotile-$2M_{c1}$ fibres lying with their fibre axes ($x$) parallel to the lizardite apparent-fibre axes ($z$). In places the lizardite stacks of plates are dominant, but overall the bastites seem to consist of more fine-grained serpentine than lizardite apparent fibres or parallel chrysotile fibres. Cutting through the bastites are cross-fibre chrysotile-$2M_{c1}$ veins in which the fibre axes always lie parallel to the fibre axes of the lizardite and chrysotile in the bastite, despite irregularities in the shape of the vein walls. Parallel growth between fibres in these veins and bastites has also been reported by Wicks & Whittaker (1977).

The amphibole bastites in specimen 18509 consist of clinoamphibole in which serpentinization has occurred along cross-cutting fractures, cleavages and grain boundaries. On the electron-microscope scale the shapes of the serpentine–amphibole boundaries seem unrelated to any particular crystallographic directions, dislocations or any other features in the amphibole. All boundaries examined in the electron microscope can be seen in the polarizing microscope to follow fairly irregular cross-cutting fractures or grain boundaries. The interfaces are not per-
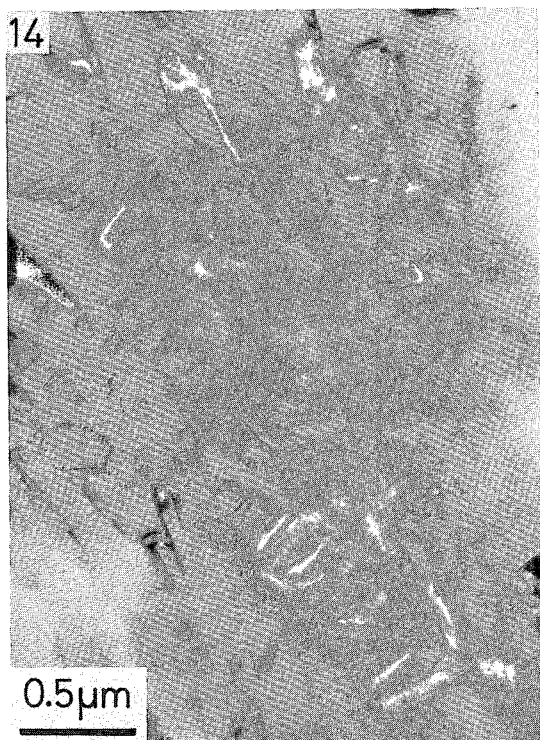
FIG. 14. Bastite, probably after clinopyroxene, in which serpentinization has been complete. Specimen 18500.
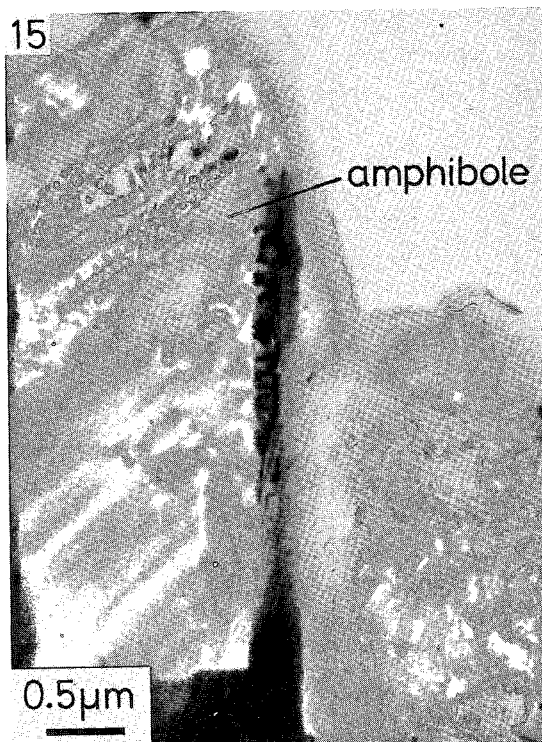
FIG. 15. An amphibole–serpentine boundary. Specimen 18509.

fectly sharp but usually consist of an indistinct zone of about 0.05 to 0.1 $\mu$m in width. In every example seen in the electron microscope all the serpentine within a few microns of the boundary is very fine-grained and featureless (Fig. 15), producing ring-type electron-diffraction patterns that cannot be identified precisely. Further from the boundary the serpentine may become coarser and more clearly crystalline, forming lizardite–$1T$ apparent fibres like those in the $\alpha$-mesh textures, in which the apparent-fibre axes ($z$) are roughly perpendicular to the boundary.

One zone of specimen 18543 contains large, partly serpentinized biotite grains. In the electron microscope the biotite contains very fine-grained, randomly oriented serpentine that cannot be identified further but that occurs in parallel bands several microns wide; this alteration has clearly taken place along biotite cleavage planes.

## NON-PSEUDOMORPHIC TEXTURES

Of the four specimens examined containing non-pseudomorphic textures, two (18523 and 18558) consist of antigorite, one (18541) consists of chrysotile with brucite and one (18543) of chrysotile and lizardite with chlorite.

## Antigorite

The antigorites were only examined briefly, but several interesting features were observed; further investigations by electron microscopy should lead to a clearer understanding of these structures. The two specimens resemble one another. A typical area of the antigorite interpenetrating texture in specimen 18558 is shown in Figure 16. Grains are generally irregular in shape and randomly oriented, though in the $\gamma$-hourglass textures, blades exhibit a stronger parallelism, with the $y$ axis parallel to the direction of elongation. Boundaries between grains are often straight or sometimes crenulated, and commonly they consist of a narrow region 0.01 to 0.02 $\mu$m wide containing amorphous or finely crystalline material.
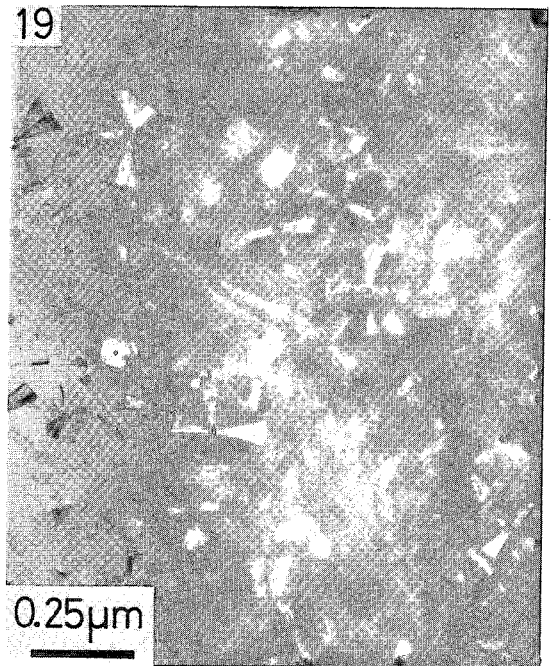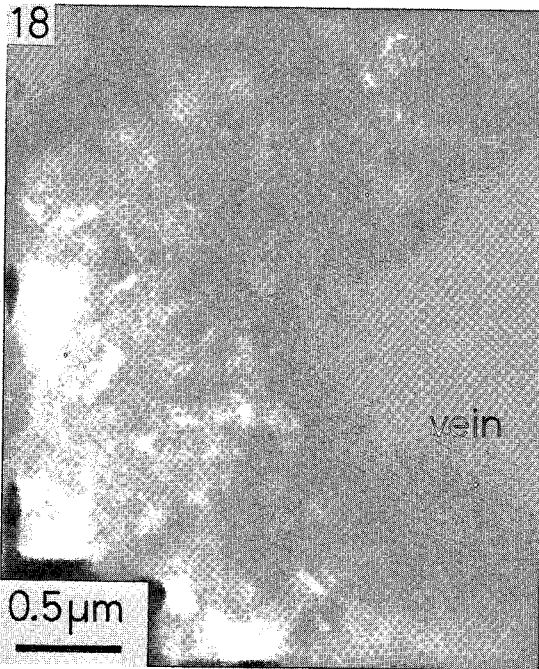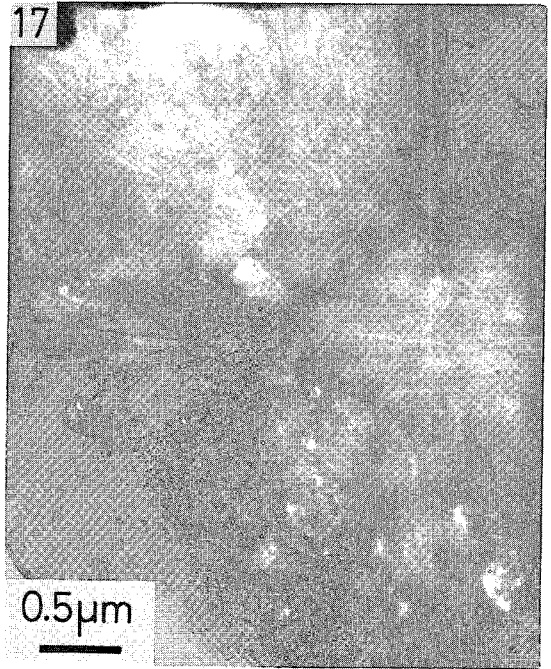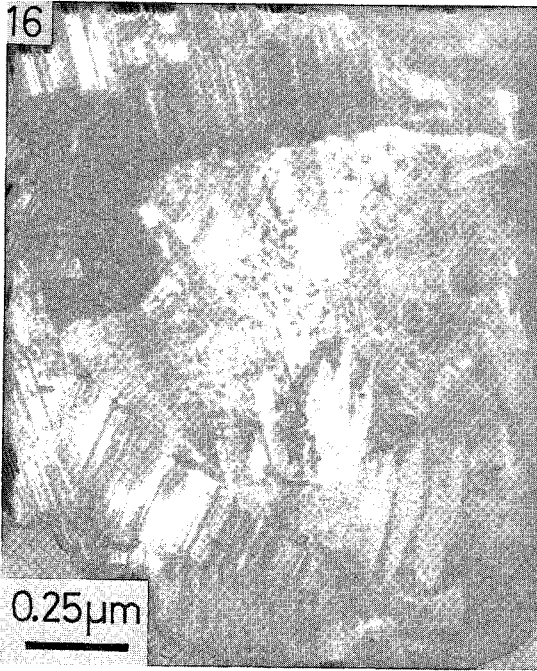
FIG. 16. Antigorite in interpenetrating textures. Specimen 18558.

FIG. 17. Chrysotile and polygonal serpentine in interpenetrating textures. Specimen 18541.

FIG. 18. Margin of a chrysotile-asbestos vein. Specimen 18540.

FIG. 19. Serpentine in an apparently non-fibrous vein. Specimen 18527.

*Chrysotile and lizardite*

The interpenetrating textures of specimen 18541 consist mainly of chrysotile–$2M_{c1}$ together with significant amounts of polygonal serpentine (Fig. 17). The fibres occur in bundles, typically a few microns wide but quite variable in size. The bundles are irregular in shape and randomly oriented, and boundaries between adjacent bundles are poorly defined. Some areas consist mainly of irregularly shaped, randomly oriented lizardite plates, but such areas are generally small and do not occur commonly. Fine-grained, poorly crystalline serpentine is also quite common. Brucite occurs in this zone, and is very similar in appearance to the brugnatellite in specimen 18505. Intergrown with the brucite, along the basal cleavages, are irregularly spaced, roughly parallel bands or lenses of chrysotile–$2M_{c1}$ fibres. These bands are generally 0.5 to 1.5 $\mu$m wide, and are irregular in shape.

The interlocking textures in specimen 18543 are composed mainly of fine-grained lizardite + chrysotile mixtures. Grain shapes are irregular and orientations are random. In addition to the serpentine there are many small areas of chlorite. Like the serpentine it is randomly oriented and is distributed fairly evenly throughout this zone of the specimen.



Fig. 20. A radial bundle of lizardite laths from the margin of a complex banded vein. Specimen 18515.

SERPENTINE VEINS

Several serpentine veins, both asbestiform and non-asbestiform, were examined. The asbestos veins are mainly cross-fibre (18500, 18540, 18541, 18543), but one slip-fibre vein (18536) was also examined. Both types are composed of parallel fibres of chrysotile–$2M_{c1}$. Generally fairly straight, the vein edges may be quite irregular (Fig. 18), though in either case the vein–matrix boundaries are always quite sharp and the veins are easily distinguishable from other textural units.

One simple fracture-filling, apparently non-fibrous vein was examined (18527). It consists of chrysotile–$2M_{c1}$ and polygonal serpentine fibres that are generally randomly oriented, although within small regions orientations may be less random, as shown in Figure 19.

A wide, complex, banded serpentine vein was also examined (specimen 18515; Wicks & Whittaker 1977, p. 474, Fig. 7c). A narrow central band consists of parallel chrysotile–$2M_{c1}$ fibres, but the main part of the vein consists of randomly oriented chrysotile–$2M_{c1}$ and polygonal serpentine fibres and minor amounts of irregularly shaped lizardite–$1T$ grains. The relative abundance of these constituents varies from place to place, and this variation does not seem to be systematic. The marginal bands of this vein, however, consist mainly of lizardite–$1T$. In the two-dimensional sections seen in the transmission electron-microscope, the lizardite appears to form roughly circular bundles of radially arranged blades (Fig. 20); in every blade x is parallel to its largest dimension (i.e., the radius of the bundle) and z is parallel to its shortest (i.e., tangential) dimension. Bundles are generally 5 to 15 $\mu$m in diameter, and may occur either in groups in which they seem to show evidence of interference during growth, or separately, surrounded by a matrix of fine-grained lizardite and chrysotile. Bundles consist of a few main laths about 0.1 to 0.2 $\mu$m in width, and from each of these extend many smaller laths, arranged fairly symmetrically as branches on either side of the main lath. These secondary laths also appear to branch into still smaller laths (about 0.01 to 0.02 $\mu$m wide), though these are less perfectly developed, arranged and distributed about the secondary
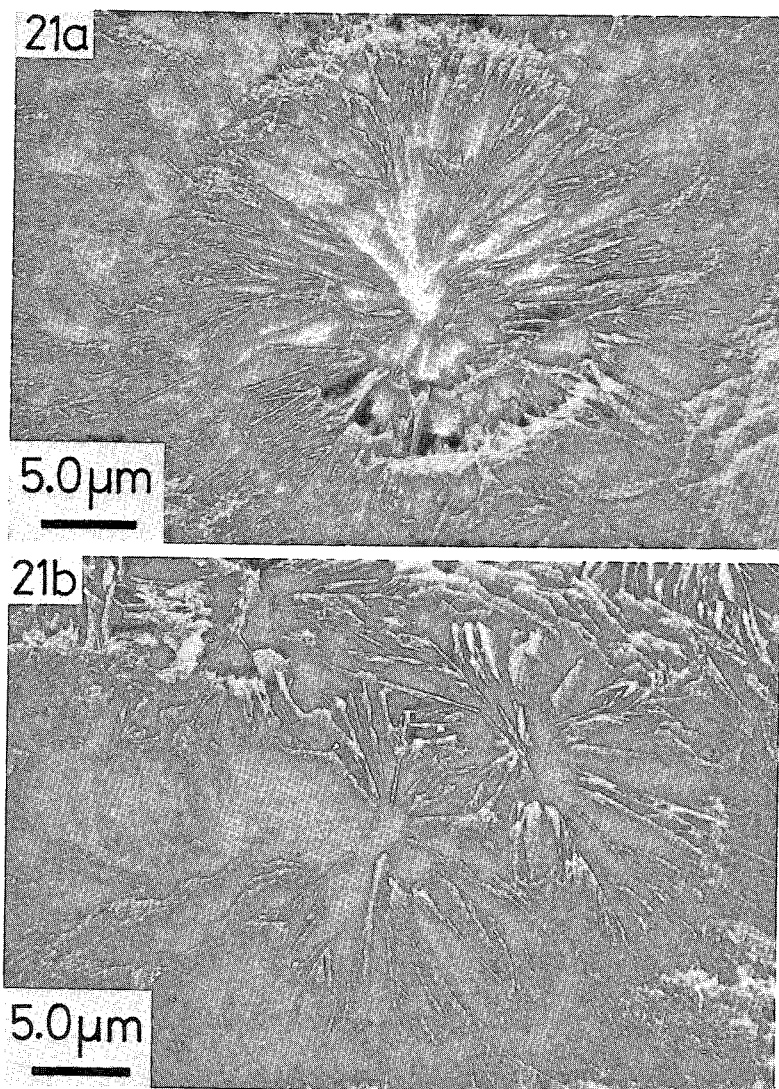
FIG. 21. Scanning electron micrographs of a region similar to that shown in Fig. 20. (a) A radial bundle of lizardite laths surrounded by fine-grained serpentine. (b) A group of bundles showing secondary branching of laths and growth interference.

laths. Among the finest laths, isolated chrysotile fibres can sometimes be seen, though these do not seem part of the structure. Scanning electron-microscopy (Fig. 21) shows that the "blades" are also elongate in the direction of the bundle axis (*i.e.,* the y-axis direction) and so would more accurately be described as plates. The observation that these plates have the z axis parallel to their shortest dimension is to be expected, considering the sheet structure of lizardite. These lizardite structures closely resemble spherulites in polymers, but are cylindrical, not spherical, in three dimensions.

## DISCUSSION

Although only a limited number of specimens were examined during this study, certain inferences can be drawn from the electron–optics observations concerning the nature of the serpentinization processes involved. The textures have been classified in terms of the types of processes that would be expected to produce them, according to Wicks & Whittaker (1977).

## Type 3

The lizardite mesh-textures in specimens 18505, 18509, 18510 and 18527 and the bastites in specimens 18509 and 18510 are formed by retrograde, type-3 serpentinization (Wicks & Whittaker 1977). The wide banded vein in specimen 18515 probably also belongs to this type.

In all pseudomorphic textures in which relict grains of the original minerals are present, the serpentine adjacent to the unaltered mineral is poorly crystalline and randomly oriented. Often it cannot be identified more precisely by electron diffraction, but when it can, the serpentine is usually found to be a mixture of lizardite and chrysotile. According to the mechanism suggested by Wicks & Whittaker (1977), the initial serpentine formed would be well-crystallized, well-oriented lizardite, such as that found in mesh rims, and the fine-grained, randomly oriented serpentine, as in mesh centres, would be produced by a secondary process. However, the occurrence of the fine-grained serpentine immediately adjacent to all boundaries with preserpentinization minerals suggests that this material probably represents the first serpentine formed during serpentinization. Yada & Iishi (1974) have used electron microscopy to examine the products of experimental serpentinization of olivine; in their runs, fine-grained chrysotile and, to a lesser extent, lizardite formed very quickly (within the first 30 minutes). Martin & Fyfe (1970) have investigated experimentally the rates of hydration of forsterite to serpentine and brucite. They have shown that the rates are rapid in relation to geological time, and that the rate of diffusion of water to the reaction site is almost certain to be rate-controlling in this reaction.

The well-crystallized serpentine such as that found in mesh rims was likely formed by recrystallization of the first-formed, poorly crystalline serpentine. This is contrary to the mechanism assumed by Wicks & Whittaker (1977) and raises questions as to why the recrystallization should always start from the sites at which serpentinization started, and why the orientation of the recrystallized lizardite should be related to these sites at the mesh boundaries. However, it would be compatible with the observations, as long as recrystallization started virtually simultaneously with serpentinization, and the serpentinization front advanced more rapidly than the recrystallization front (R. L. Stanton, pers. comm.). Recrystallization of lizardite would then be expected to produce apparent fibres perpendicular to the grain boundaries and fractures in the olivine as stacks built up from the passages carrying the hydrothermal fluids. If suitable conditions were maintained until the whole of the original serpentine had recrystallized, an hourglass texture could be observed; if conditions were suitable for a shorter length of time, then narrow rims would form, leaving much serpentine unrecrystallized in mesh centres. In this study, mesh textures containing relict olivine have been found in which the mesh rims closely surround the olivine. If the mechanism suggested here is correct, it is likely that in some mesh textures containing only small amounts of relict olivine the recrystallization of serpentine was not complete and wider regions of poorly formed serpentine lie between the olivine and the mesh rims. Mesh cells such as these were not observed during this limited study. The sharpness of the rim–centre boundaries suggests that the growth-rate curve for this recrystallization may drop sharply at a critical condition. Possibly the same is true in the case of chrysotile mesh-textures, but the relative scarcity of these suggests that more special conditions are required for the formation of chrysotile mesh-textures than of those made up of lizardite. (Specimen 18501 is thought to have been formed by type-5 processes; see below.) Though some chrysotile is usually present in lizardite mesh-centres, none is found in lizardite mesh-rims. This is perhaps surprising since chrysotile has a more highly ordered structure than lizardite. In chrysotile mesh-textures, chrysotile and polygonal serpentine form the mesh centres, but chrysotile alone forms the rims. (Although Wicks (1969) has reported traces of lizardite in these rims, none was found in this study.)

With these observations, it would seem more likely that the mechanism postulated here for the production of mesh and hourglass textures is correct, and that the mechanism suggested by Wicks & Whittaker (1977), in which serpentinization of olivine should produce well-crystallized, oriented lizardite mesh-rims by a steadily advancing serpentinization front, is incorrect. According to the mechanism suggested by these authors, serpentine mesh-centres would be produced as the reaction front stops and the remnant olivine undergoes serpentinization simultaneously throughout the grain, producing fine-grained, randomly oriented serpentine. It is difficult to visualize how serpentinization could take place other than by a fairly steadily advancing reaction-front, as the alteration has to be hydrothermal. Dungan (1977) has sug-

gested that mesh rims form while the supply of fluid for the reaction is steady. Then at some point the supply channels are sealed by serpentine; mesh centres form when the fluid supply is impeded. However, such a change would likely be gradual, and would not be expected to produce the sharp rim–centre interfaces observed consistently throughout this study.

The lizardite hourglass textures in specimens 18540 and 18500 are also type-3 retrograde pseudomorphic textures, but both are in asbestos deposits associated with type-5 prograde textures; it could be argued that they represent the early stages of the process of recrystallization from type 3 to type 5.

In bastites, recrystallization of the first-formed, poorly crystalline serpentine might be expected to form apparent fibres growing perpendicular to nucleation sites on exsolution lamellae interfaces, as is suggested by the observed (albeit poorly developed) relationship in crystallographic orientations between serpentine and pyroxene. The presence of polygonal serpentine nucleated on the edges of exsolution lamellae in pyroxene among the fine-grained serpentine (Fig. 12) is interesting. In this, $x_{serpentine}$ is parallel to $z_{pyroxene}$, but being semicircular in section, both [010] and [001] serpentine directions lie perpendicular to the lamellar interface. This structure must be destroyed if the serpentine recrystallizes completely in the manner suggested above. In the absence of exsolution lamellae, apparent fibres might grow perpendicular to cleavages, as seems to be the case in the amphibole bastites, or along the cleavages, as suggested by the observations on a completely serpentinized pyroxene bastite (18500). However, in the latter specimen, the fact that the serpentine in the veins cutting the bastite has its fibre axes parallel to those of the lizardite and chrysotile in the bastite suggests that in some cases, conditions other than the habit or structure of the original mineral may control the orientation of the serpentine in a pseudomorphic texture. In this case the forces causing the orientation of the chrysotile in the fracture-filling vein may also have controlled the orientation of recrystallized serpentine in the bastite. This specimen, from an asbestos deposit, probably represents a type-3 texture which has undergone partial recrystallization to type 5.

The presence of magnetite and brugnatellite in some mesh centres is consistent with the interpretation that mesh rims are produced by recrystallization. During the recrystallization it is likely that impurities would be pushed in-

ward by the advancing reaction-front, unless conditions were such that they could migrate right out of the textural units. As has been suggested by various authors (see review by Moody 1976), magnetite probably forms from the iron in excess of that which can be taken into the serpentine structure when a ferromagnesian mineral is altered. Also, the brugnatellite analyzed by electron microprobe during this study (Cressey 1977) was found to have a much higher Fe:Mg ratio than the serpentine. Brugnatellite contains large amounts of $H_2O$ and some $CO_2$ in its structural formula; this brugnatellite also contains a significant amount of Cl. Its composition may reflect the nature of the hydrothermal fluid involved in serpentinization, and its presence may be due to special conditions that have allowed some of the ions in the fluid to be trapped in the rock instead of being carried right out of it, as they usually seem to be. This is consistent with the mechanism for alteration of ultramafic rocks, involving Cl, suggested by Rucklidge (1978). However, the brugnatellite may instead be associated with the alteration of serpentine to carbonates and talc, and therefore not be related to serpentinization.

The interesting structure found in the margins of the complex vein (18515) has not been observed in any other texture examined during this study; thus it could probably only form under the special conditions found in the margins of such a vein. Plagioclase has been observed to form structures very similar in appearance to this, though on a larger scale, in chilled margins of basic intrusions. Although crystallization in an intrusion of magma and in a hydrothermal vein obviously involves quite different processes, special conditions may occur in each of these situations (e.g., high nucleation- and growth-rates producing skeletal-type structures, then rapid quenching) to produce these unusual crystal-shapes and arrangements.

*Type 5*

The chrysotile mesh-texture in specimen 18501 and the non-pseudomorphic textures in specimens 18541 and 18543 represent prograde type-5 textures. Although 18501 bears some similarities to the lizardite mesh-textures, it formed under different conditions and probably through a different mechanism, the recrystallization of lizardite rather than the alteration of olivine. It is from an asbestos deposit, as is 18543.

In the interlocking and interpenetrating tex-

tures the lizardite grains and chrysotile-fibre bundles are irregular in shape and randomly oriented. As observed by Wicks & Whittaker (1977), prograde recrystallization has obliterated the lizardite pseudomorphs after olivine, but bastites seem to be slightly more resistant. The chrysotile and lizardite in the non-pseudomorphic textures do not differ significantly from those seen in the non-recrystallized parts of the pseudomorphic textures. However, the proportion of chrysotile to lizardite is much greater in the non-pseudomorphic textures than in the pseudomorphic textures.

Experimental studies have not clearly defined the stability fields of chrysotile and lizardite, but field evidence (Wicks 1969, Mumpton & Thompson 1975) suggests that chrysotile tends to become dominant over lizardite as one moves from low- to high-metamorphic-grade serpentinites. Antigorite becomes dominant over both chrysotile and lizardite in the upper-greenschist–lower-amphibolite facies (Evans & Frost 1975).

The presence of brucite in specimen 18541 can possibly be explained in a way similar to the case of brugnatellite in one of the pseudomorphic textures. Like the brugnatellite, brucite also has a higher Fe:Mg ratio than serpentine (Cressey 1977). This has also been found by previous workers (see review by Moody 1976). Possibly the presence of fine-grained chlorite may also be explained by a similar argument. However, some of the chlorite seen in the optical microscope is obviously a preserpentinization phase, and possibly the small, randomly oriented grains of chlorite intergrown with serpentine could represent a recrystallization of original chlorite, just as pseudomorphic serpentine is recrystallized to form non-pseudomorphic textures.

*Type 7*

The antigorite interpenetrating textures in specimens 18523 and 18558 represent prograde, type-7 serpentinization. The antigorite grains are irregular in shape and randomly oriented. In both specimens antigorite is the only mineral present. No traces of pseudomorphic textures remain; the apparent hourglass textures in specimen 18558 are not thought to be related to the original rock-texture but have probably been formed by interference during growth of the antigorite blades.

### ACKNOWLEDGEMENTS

### REFERENCES

BARBER, D.J. (1970): Thin foils of non-metals made for electron microscopy by sputter-etching. *J. Mat. Sci.* 5, 1-8.

CHAMPNESS, P.E. & LORIMER, G.W. (1971): An electron microscopic study of a lunar pyroxene. *Contr. Mineral. Petrology* 33, 171-183.

CRESSEY, B.A. (1977): *Electron Microscopic Studies of Serpentinites.* Ph.D. thesis, Manchester Univ., Manchester, England.

———— & ZUSSMAN, J. (1976): Electron microscopic studies of serpentinites. *Can. Mineral.* 14, 307-313.

DUNGAN, M.A. (1977): Metastability in serpentine – olivine equilibria. *Amer. Mineral.* 62, 1018-1029.

EVANS, B.W. & FROST, B.R. (1975): Chrome–spinel in progressive metamorphism – a preliminary analysis. *Geochim. Cosmochim. Acta* 39, 959-972.

MARTIN, B. & FYFE, W.S. (1970): Some experimental and theoretical observations on the kinetics of hydration reactions with particular reference to serpentinization. *Chem. Geol.* 6, 185-202.

MOODY, J.B. (1976): Serpentinization: a review. *Lithos* 9, 125-138.

MUMPTON, F.A. & THOMPSON, C.S. (1975): Mineralogy and origin of the Coalinga asbestos deposit. *Clays Clay Minerals* 23, 131-144.

RUCKLIDGE, J.C. (1978): The enigmatic role of Cl in the alteration of ultramafic rocks. *Int. Mineral. Assoc. Gen. Meet. (Novosibirsk) Program* 1, 44 (Abstr.)

———— & ZUSSMAN, J. (1965): The crystal structure of the serpentine mineral, lizardite, $Mg_3Si_2O_5(OH)_4$. *Acta Cryst.* **19**, 381-389.

WICKS, F.J. (1969): *X-ray and Optical Studies on Serpentine Minerals*. D.Phil. thesis, Univ. Oxford, Oxford, England.

———— & WHITTAKER, E.J.W. (1975): A reappraisal of the structures of the serpentine minerals. *Can. Mineral.* **13**, 227-243.

———— & ———— (1977): Serpentine textures and serpentinization. *Can. Mineral.* **15**, 459-488.

————, ———— & ZUSSMAN, J. (1977): An idealized model for serpentine textures after olivine. *Can. Mineral.* **15**, 446-458.

———— & ZUSSMAN, J. (1975): Microbeam X-ray diffraction patterns of the serpentine minerals. *Can. Mineral.* **13**, 244-258.

YADA, K. & IISHI, K. (1974): Serpentine minerals hydrothermally synthesized and their microstructures. *J. Crystal Growth* **24/25**, 627-630.